Earth Syst. Sci. Data Discuss., 4, 123–139, 2011
www.earth-syst-sci-data-discuss.net/4/123/2011/
doi:10.5194/essdd-4-123-2011

Open Access Earth System Science Data Discussions

King George Island ice cap geometry updated with airborne GPR measurements

M. Rückamp[1,*] **and N. Blindow**[2]

[1]Institute for Geophysics, University of Münster, Corrensstraße 24, 48149 Münster, Germany
[2]Federal Institute for Geosciences and Natural Resources, Stilleweg 2, 30655 Hannover, Germany
[*]present address: Institute for Geophysics, KlimaCampus, University of Hamburg, Bundesstraße 55, 20146 Hamburg, Germany

Received: 15 November 2011 – Accepted: 16 November 2011 – Published: 8 December 2011

Correspondence to: M. Rückamp (martin.rueckamp@zmaw.de)

Published by Copernicus Publications.

Abstract

Ice geometry is a mandatory requirement for numerical modelling purposes. In this paper we present a consistent data set for the ice thickness, the bedrock topography and the ice surface topography of the King George Island ice cap (Arctowski Icefield and the adjacent central part). The newly data set is composed of groundbased and airborne Ground Penetrating Radar (GPR) and differential GPS (DGPS) measurements, obtained during several field campaigns. Blindow et al. (2010) already provided a comprehensive overview of the groundbased measurements carried out in the safely accessible area of the ice cap. The updated data set incorporates airborne measurements in the heavily crevassed coastal areas. Therefore, in this paper special attention is paid to the airborne measurements by addressing the used instrument, survey, and data processing in more detail. In particular, the inclusion of airborne GPR measurements with the 30 MHz BGR-P30-System developed at the Institute of Geophysics (University of Münster) completes the picture of the ice geometry substantially. The compiled digital elevation model of the bedrock shows a rough, highly variable topography with pronounced valleys, ridges, and troughs. Mean ice thickness is ~240 m, with a maximum value of ~400 m in the surveyed area. Noticeable are bounded areas in the bedrock topography below sea level where marine based ice exists. The provided data set is required as a basis for future monitoring attempts or as input for numerical modelling experiments. The data set is available from the PANGAEA database at doi:10.1594/PANGAEA.770567.

1 Introduction

King George Island (KGI) is the largest of the South Shetland Islands (SSI) situated at the northern tip of the Antarctic Peninsula (Fig. 1). Due to their small size and and geographical location in maritime climate conditions, the ice caps of the SSI are regarded as to be temperate (ice temperatures at or close to pressure melting point conditions);

ESSDD
4, 123–139, 2011

meltwater may be present within the ice body (Paterson, 1994). More than 90 % of the KGI is glaciated and the main ice domes rise up to 700 m. Blindow et al. (2010) provided the most detailed picture so far of the ice surface and the bedrock topography as well as the ice thickness distribution of the KGI ice cap. In their study, the geometry information was derived from groundbased Ground Penetrating Radar (GPR) and Differential GPS (DGPS) profile measurements in the safely accessible uncrevassed areas. The GPR measurements were carried out during austral summer 1997/98 and 2006/07. The monopulse GPR equipment used was a proprietary construction of the University of Münster (Germany). They successfully operated at center frequencies of 25 MHz and 50 MHz with regard to detection of the bedrock topography at this ice cap. The choice for low frequency GPR Systems was made to overcome scattering effects and absorption of temperate ice (e.g. Ewen Smith and Evans, 1972). However, the work lacks in coverage of the heavily crevassed coastal areas. During a field campaign in austral summer 2008/09 we applied an airborne GPR system in the northwestern coastal areas to achieve a more complete picture of the ice geometry. This paper describes the airborne GPR system we used, the airborne GPR survey as well as the corresponding data processing and integrates these data into the already existing data set from Blindow et al. (2010).

2 Methods

2.1 GPR System

An airborne GPR system was used to measure ice thickness in inaccessible, crevassed coastal areas of the ice cap. This 30 MHz monopulse system was developed at the University of Münster (Germany) and was named UMAIR (University of Münster Airborne Ice Radar) until the end of 2009. The system was then purchased by BGR (Federal Institute for Geosciences and Natural Resources, Germany) and is now operating as BGR-P30 in geological and glaciological projects. The radar consists of a shielded

ESSDD
4, 123–139, 2011

broadband antenna system with integrated electronics for downward transmission of the 30 MHz wavelet and reception of upgoing reflected waves. At the receiving antenna the signals are directly A/D converted at a rate of 400 MHz with 4096 points per trace, stacked 256 times and then routed via fibre optic cables to the control unit in the helicopter cabin. At 10 Hz data acquisition rate and 35 kn average helicopter cruising speed ~500 traces per kilometer are recorded. For more details about the radar system BGR-P30 see Blindow (2009), Eisenburger et al. (2009), and Blindow et al. (2011).

2.2 GPR Survey

Figure 2 shows the spatial distribution of the groundbased GPR profiles and the airborne GPR profiles. As shown in Blindow et al. (2010), the groundbased survey with a length of about 1200 km covered an area of ~200 km^2 of the Arctwoski Icefield, the adjacent Central Part, and the exposed located Bellingshausen Dome with a total length of about 1200 km. At the Arctowski Icefield the grid was orientated in northwest-southeast direction with a grid spacing of 1000 m between the profiles; on the Central Part the survey was arranged in north-south direction with a spacing of 500 m. These grids were designed to have a large number of crossover check points.

For the northwestern areas of the Arctowski Icefield and the Central Part, the total airborne GPR survey length is 250 km with an estimated coverage of 140 km^2. The grid spacing between the northwest-southeast orientated profiles is ~700 m. The airborne flight lines were designed in order to connect continuously to the groundbased GPR survey. The flight was realized with a Sikorsky UH-60 Black Hawk utility helicopter with the GPR antenna as hanging load (the helicopter was provided by FACH – Fuerza Aérea de Chile). The Black Hawk was equipped with fuel tanks which allowed to perform the flight without refueling stop. The GPR survey consisted of 53 profile sections achieved by one flight taking four hours. The average cruising speed was 35 kn (65 km h^{-1}) at 40 m average elevation of the antenna over the ground (controlled by laser altimeter). The radar profiles were located with a pair of NovAtel DLV dual frequency DGPS receivers collecting position data (x, y, z) at a sampling rate of 10 Hz.

ESSDD
4, 123–139, 2011

However, due to bad weather conditions, and therefore flight hour limitations, there are only a few crossover check points within the airborne survey as well as a limited overlap between the airborne and groundbased grids.

2.3 GPR processing and data

All airborne radar data were processed with the ReflexW program (Vers. 4.5, K.J. Sandmeier software) in several steps comprising georeferencing, a time zero correction corresponding to the antenna offset, consideration of the air layer, and a frequency domain Butterworth-Bandpass filter from 5 to 30 MHz. Time domain migration (diffraction stack) with a two layer velocity model was used to collapse diffraction hyperbolas and to recover the dip of reflectors. The two layer velocity model consisted of the air layer with a velocity of $0.3\,\mathrm{m\,ns^{-1}}$ and the ice layer with an average velocity of $0.168\,\mathrm{m\,ns^{-1}}$. To account for dielectric losses in the temperate ice a gain of $0.08\,\mathrm{dBm^{-1}}$ was applied to all traces.

The ice surface elevation z_s was obtained by subtracting the thickness of the air layer derived from the airborne GPR measurements from the measured DGPS height at the GPR antenna. Ice thickness values H were determined by converting the two-way-traveltimes (twt in ns) with an appropriate depth-dependent velocity model. Similar to Blindow et al. (2010), we used common mid point (CMP) measurements to determine the velocities of the radar signals in the subsurface. Additionally, we introduce a firn correction term to account for the spatially variable firn layer

$$H = 0.194\left[\mathrm{m\,ns^{-1}}\right] t_\mathrm{firn}/2 + \left(0.168\left[\mathrm{m\,ns^{-1}}\right] t_\mathrm{b} - t_\mathrm{firn}\right)/2 \quad (1)$$

with the firn correction term

$$t_\mathrm{firn} = \begin{cases} 1.4 \cdot z - 350\,[\mathrm{ns}] & z > 250\,\mathrm{m\ a.s.l.} \\ 0.0 & z \leq 250\,\mathrm{m\ a.s.l.}, \end{cases} \quad (2)$$

where t_firn and t_b are the twts of the firn and bedrock reflections, respectively. The firn correction represents a linear adaption to the spatially extended water table with

ESSDD
4, 123–139, 2011

varying depth marking the firn ice transition zone in the accumulation area (Blindow et al., 2010). Our GPR measurements detected the water table at a maximum depth of 40 m at 700 m a.s.l. elevation and around 25 m depth at 400 m a.s.l. Below ~250 m a.s.l. the water table disappears. The latter value represents the equilibrium line altitude (e.g. Braun and Rau, 2000). The firn ice transition zone at the higher altitudes was previously identified by Wen et al. (1994) and Simões et al. (2004). They obtained water table depths by drilling at the Arctowski Icefield around 650 m a.s.l. elevation. Our water table depth of 40 m at 700 m a.s.l. elevation coincide with their measurements.

Before merging the different data sets we collected during several expeditions, we have to mention that the ice surface topography is not in balance (Rückamp et al., 2011). At Bellingshausen Dome below 250 m a.s.l., significant height changes have been measured in the eleven year period (up to 1.44 m a^{-1} at 20 m a.s.l.). As we surveyed Bellingshausen Dome on a very dense grid in 2008/09 (Rückamp et al., 2011), we simply dropped measurements from former expeditions. All other low elevation areas (margins of the ice cap) were measured in a single airborne survey in the same year. Measurements in areas above 250 m a.s.l. do not require corrections in case of multiple readings in different years. In these areas ice thickness and hence bedrock topography do not show significant changes within a decade. Therefore, the compiled data set refers to the 2008/09 austral summer.

Comparative ice thickness values and ice surface heights at each crossover check points of the airborne and groundbased radar profiles were calculated to estimate the vertical accuracy of the compiled data set (similar to the crosspoint analysis described in Rückamp et al., 2011). The crosspoint analysis yields in a vertical accuracy in meter range or less for the ice thickness (lower than half the wavelength in ice $\lambda/2$). Therefore, we assume a relative error of about ±2.3 % for the ice thickness H.

The estimated vertical accuracy of the ice surface topography is about ±6 cm for the groundbased measurements (a few thousands of crossover check points). However, some points of comparison, located at the glaciated margins (Bellingshausen Dome), show differences in meter range. These differences are attributed to melt processes

ESSDD
4, 123–139, 2011

as the season progresses. For the airborne measurements with less crossover check points we calculated a mean accuracy of ±1 m where the maximum difference is 3 m. This poorer accuracy is attributed to the rough (heavily crevassed) surface.

An example of a processed and topographically corrected airborne radar-data obtained in the transition zone from the Arctowski Icefield to the Central Part can be seen in Fig. 3. The profile shows the water table, the bedrock and internal scattering. The ice surface is smooth whereas the bedrock is rough with carved valleys.

3 Results

After merging the data sets, we included an already existing ice surface topography data set for the Admiralty Bay available via SCAR KGIS (Braun et al., 2001). Furthermore we added the coast line (taken from Rückamp et al., 2011) with values of 0 m for the ice thickness except for the airborne surveyed areas. The spatially unstructured data set along the profiles was then gridded using the kriging algorithm on a 250 m grid for the ice surface topography z_s and ice thickness H. Subtracting the ice thickness grid from the ice surface grid, we obtain a grid for the bedrock topography z_b. With these data sets we constructed digital elevation models (DEM) for the ice surface and bedrock topography as well as a map of the ice thickness distribution.

3.1 Ice thickness map

Figure 4 shows the composed interpolated ice thickness distribution H (m) in the investigated area. The maximum ice thickness on the profiles is 422 m measured at the Central Part; at Arctwoski Icefield the maximum value is 397 m. These listed values remained unchanged compared to Blindow et al. (2010) whereas the newly calculated mean ice thickness along the profiles with 238 m is slightly lower. This reduced value is explained by the in general lower ice thickness values in the coastal areas compared to the inner parts. However, along the airborne profiles we found a maximum ice

ESSDD
4, 123–139, 2011

thickness value of 412 m located in the transition zone from the Arctowski Icefield to the Central Part. Using the interpolated grids, the ice volume of the investigated area was calculated to 88.2 km^3 on an area of 465 km^2. As mentioned by Blindow et al. (2010) some southeast to northwest striking areas of thick ice are clearly visible and indicate the main drainage valleys of the ice cap. These features are particularly evident in the airborne surveyed area of the Central Part. These drainage characteristic can also be seen in the bedrock topography (see paragraph below). The smooth contours e.g. near the Admiralty Bay coast, are an extrapolation artefact.

3.2 DEM of the surface topography

The DEM of the composed interpolated ice surface topography z_s is shown in the Fig. 5. Compared to Blindow et al. (2010) the main pattern of the ice surface topography remained unchanged: the Arctwoski Icefield shows the dominating two domes with maximum heights of 702 m and 650 m; the highest elevation of 727 m is reached at the Dome lying in the Central Part. The exposed located Bellingshausen Dome reveals a height at the summit of 265 m. However, the airborne measurements reveal some structures in the coastal ice surface topography, e.g. a distinct ridge (interpreted as ice divide) in the Central Part in southeast-northwesterly direction.

3.3 DEM of the bedrock topography

The calculated DEM of the bedrock topography is displayed in Fig. 6. Following the description of Blindow et al. (2010), the bedrock topography reflects the geological situation described in Birkenmajer (1997): an uplifted unit called Barton Horst and a lower area named Fildes Block. In the updated picture that situation is clearly apparent.

The highly variable bedrock topography reflects steep valleys pointing northwestwards. Spatially, these valleys correlate with areas of maximum ice thickness. The already mentioned, pronounced ridge in the ice surface topography at the Central Part

ESSDD
4, 123–139, 2011

is also quite evident in the bedrock topography. This ridge may divide the Central Part into different catchments.

Another important feature is detected by the airborne measurements: Considering a constant offset of 21 m between the WGS84 ellipsoidal height and the orthometric height (using the EGM 2008 model, where the WGS84 ellipsoidal height is above the orthometric height, Pavlis et al., 2008), distinctive areas below the current sea level appear in the bedrock topography. These areas are visualized in Fig. 6 (white thick line). Especially the Central Part exhibits large areas below sea level with a maximum depth of −91 m.

4 Conclusions

We provide a consistent ice geometry data set for the King George Island ice cap. The already existing picture derived from groundbased GPR was updated with an airborne GPR survey filling the data gaps, especially close to the crevassed coastal areas. However, the presented work still lacks in measurements for the Eastern Part of the island. This can be overcome by additional flights. Due to steep surface slopes, larger crevassed areas, and a more difficult approach from a research station groundbased measurements are much more expensive at these part of the island. Additionally, this work demonstrates impressively that airborne GPR measurements (with the BGR-P30-System) are a fast and time effective tool for mapping, in particular, in crevassed areas.

The available data set may be used for/as

- reference for future monitoring and for long-term measurements to detect a response of the glacier to changing climate. Glacial thinning and retreat of calving fronts at the glaciated margins are already evident and linked to the observed regional warming (Simões et al., 1999; Rückamp et al., 2011);
- including these ice volume measurements in the World Glacier Inventory (WGI) of Glaciers and Ice Caps (GIC). The need of these measures were emphasized by

ESSDD
4, 123–139, 2011

e.g. Radić and Hock (2010) to reduce uncertainties as these regions are poorly inventoried;

– numerical modelling studies either diagnostic or prognostic to enhance the knowledge of the current and future glacial state of this ice cap (e.g. Rückamp et al., 2010).

Acknowledgements. The airborne measurements would have never been possible without the particular efforts and support by FACH (Fuerza Aérea de Chile), especially by C. Madina. The authors would like to thank the German, Chilean, and Uruguayan Antarctic Programs for their logistic support. The crew of Artigas station provided a warm and pleasant environment during the fieldwork. The collaboration and fieldwork with S. Suckro (AWI Bremerhaven, Germany) and B. Boemer, H. Knese, S. Ueding, (University of Münster, Germany) is kindly acknowledged. The German Research Foundation funded this study under grant BL307-1/2.

References

Birkenmajer, K.: Geology of the northern coast of King George Island, South Shetland Islands (West Antarctica), Stud. Geol. Polon., 110, 7–26, 1997. 130

Blindow, N.: The University of Münster Airborne Ice Radar (UMAIR): Instrumentation and first results of temperate and polythermal glaciers, in: Proc. 5th International Workshop on Advanced Ground Penetrating Radar, Granada, Spain, 28–30, 2009. 126

Blindow, N., Suckro, S., Rückamp, M., Braun, M., Schindler, M., Breuer, B., Saurer, H., Simões, J. C., and Lange, M.: Geometry and status of the King George Island ice cap (South Shetland Islands, Antarctica), Ann. Glaciol., 51, 103–109, 2010. 124, 125, 126, 127, 128, 129, 130, 135, 137, 138, 139

Blindow, N., Salat, C., Gundelach, V., Buschmann, U., and Kahnt, W.: Performance and calibration of the helicopter GPR system BGR-P30, in: Proceedings of the 6th International Workshop on Advanced Ground Penetrating Radar (IWAGPR 2011), Aachen, Germany, 153, 1–5, doi:10.1109/IWAGPR.2011.5963896, 2011. 126

Braun, B., Simões, J. C., Vogt, S., Bremer, U. F., Pfender, M., Saurer, H., Aquino, F. E., and Ferron, F. A.: An improved topographic database for King George Island: compilation, application and outlook., Antarct. Sci., 13, 41–52, doi:10.1017/S0954102001000074, 2001. 129

ESSDD
4, 123–139, 2011

Braun, M. and Rau, F.: Using a multi-year data archive of ERS SAR imagery for the monitoring of firn line positions and ablation patterns on the King George Island ice cap (Antarctica), Dresden FRG, 2000. 128

Eisenburger, D., Blindow, N., Suckro, S., Lentz, H., Krellmann, Y., and Triltzsch, G.: Helicopter borne GPR systems for geological applications: pulse radar and stepped frequency radar in gating mode, in: Proceedings of the 5th International Workshop on Advanced Ground Penetrating Radar (IWAGPR 2009), Granada, Spain, 83–87, 2009. 126

Ewen Smith, B. M. and Evans, S.: Radio-echo sounding: absorption and scattering by water inclusions and ice lenses, J. Glaciol., 11, 133–146, 1972. 125

Paterson, W. S. B.: The Physics of Glaciers, Pergamon Press, Oxford, England, 3rd edn., 1994. 125

Pavlis, N. K., Holmes, S. A., Kenyon, S. C., and Factor, J. K.: An Earth Gravitational Model to Degree 2160: EGM2008, European Geosciences Union General Assembly, Vienna, Austria, 13–18 April 2008. 131

Radić, V. and Hock, R.: Regional and global volumes of glaciers derived from statistical upscaling of glacier inventory data, J. Geophys. Res., 115, F01010, doi:10.1029/2009JF001373, 2010. 132

Rückamp, M., Blindow, N., Suckro, S., Braun, M., and Humbert, A.: Dynamics of the ice cap on King George Island, Antarctica: Field measurements and numerical simulations, Ann. Glaciol., 51, 80–90, 2010. 132

Rückamp, M., Braun, M., Suckro, S., and Blindow, N.: Observed glacial changes on the King George Island ice cap, Antarctica, in the last decade, Global Planet. Change, 79, 99–109, doi:10.1016/j.gloplacha.2011.06.009, 2011. 128, 129, 131

Simões, J. C., Bremer, U. F., Aquino, F. E., and Ferron, F. A.: Morphology and variations of glacial drainage basins in the King George Island ice field, Antarctica, Ann. Glaciol., 29, 220–224, 1999. 131

Simões, J. C., Ferron, F. A., Bernardo, R. T., Aristarain, A. J., Stiévenard, M., Pourchet, M., and Delmas, R. J.: Ice core study from the King George Island, South Shetlands, Antarctica, Pesquisa Antártica Brasileira, 4, 9–23, 2004. 128

Wen, J., Kang, J., Xie, Z., Han, J., and Lluberas, A.: Climate, mass balance and glacial changes on small dome of Collins ice cap, King George Island, Antarctica, Antarct. Res., 5, 52–61, 1994. 128

ESSDD
4, 123–139, 2011

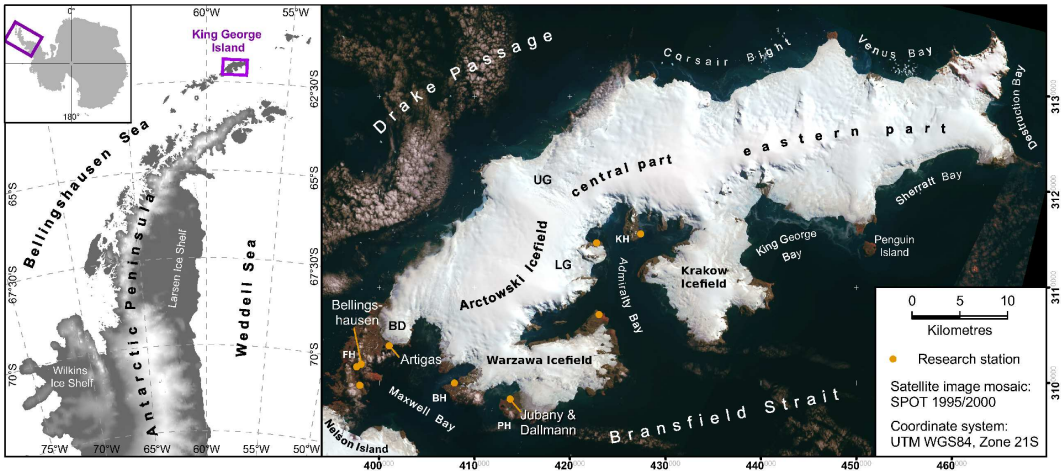

Fig. 1. Overview map of King George Island and its location on the Antarctic Peninsula. FH denotes Fildes Peninsula, BH Barton Peninsula, PH Potter Peninsula, KH Keller Peninsula, BD Bellingshausen Dome, LG Lange Glacier, and UG Usher Glacier. Background Image is a ©SPOT Image from 2000. Reprinted from the Annals of Glaciology with permission of the International Glaciological Society.

ESSDD
4, 123–139, 2011

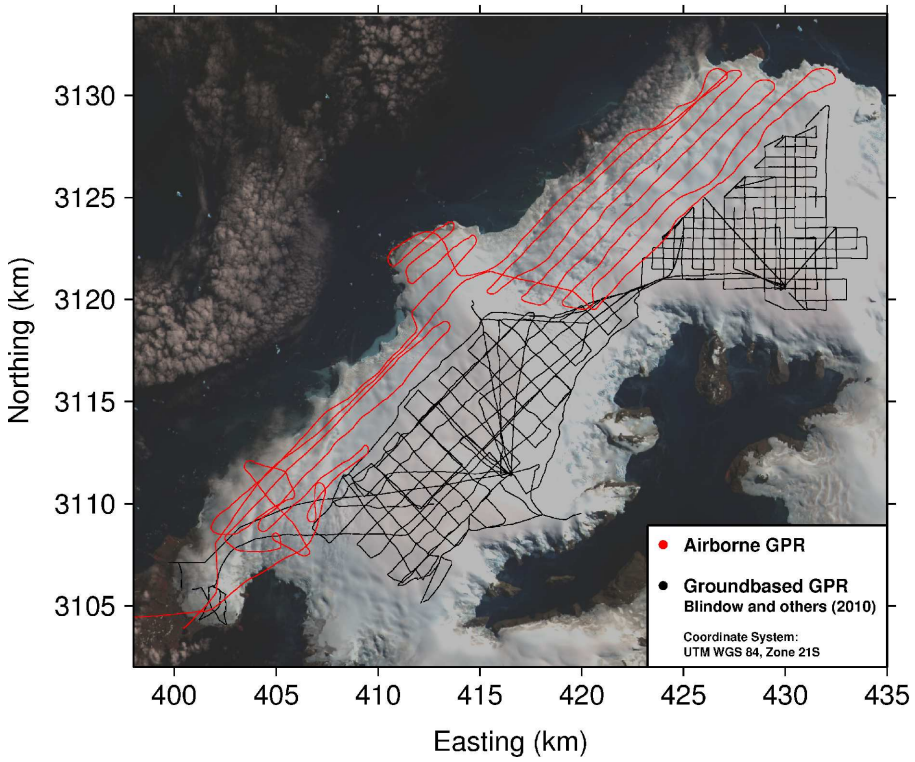

Fig. 2. Spatial distribution of the airborne GPR survey (red) and groundbased GPR survey (black; taken from Blindow et al., 2010). Background image is a ©SPOT Image from 2000.

ESSDD
4, 123–139, 2011

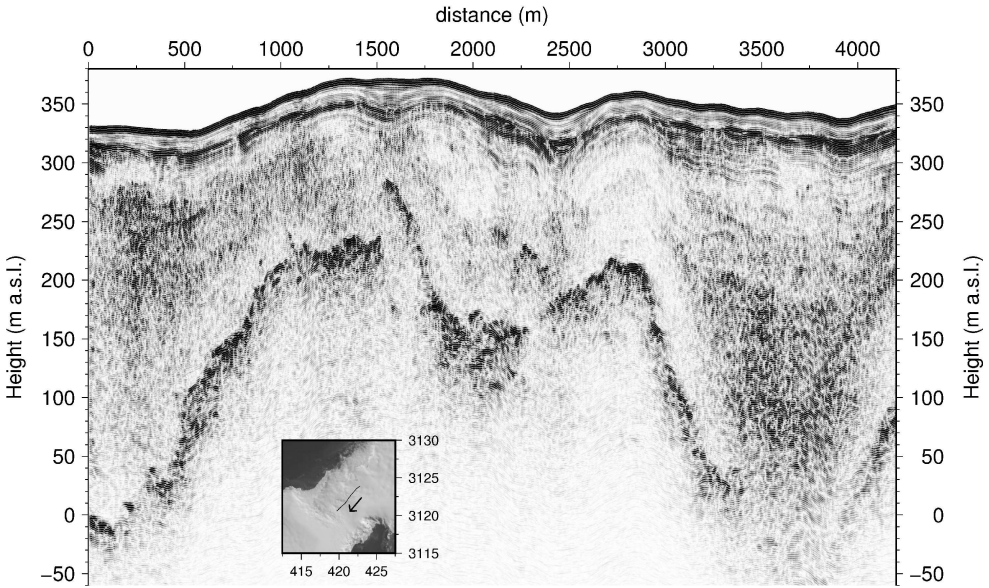

Fig. 3. Typical example of an airborne radargram. The inset shows the profile location and flight direction.

ESSDD
4, 123–139, 2011

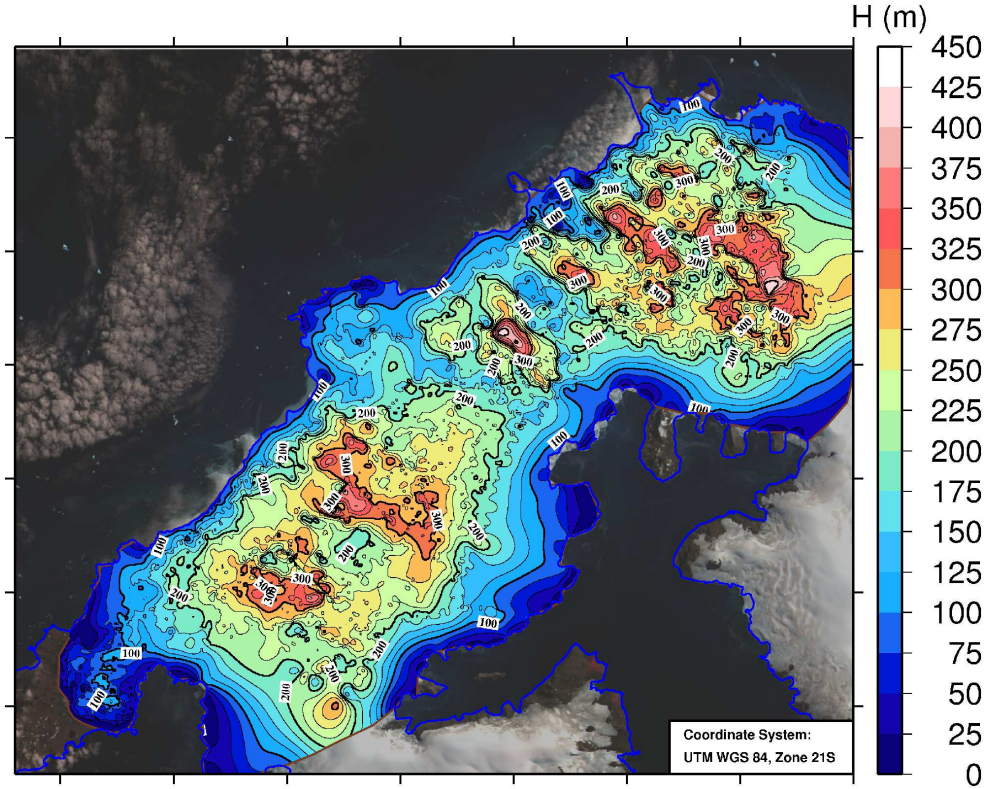

Fig. 4. Interpolated ice thickness distribution H in m on King George Island (the contour line interval is 25 m). Database: compilation of the groundbased survey (taken from Blindow et al., 2010) and the airborne measurements. Background image is a ©SPOT Image from 2000.

ESSDD
4, 123–139, 2011

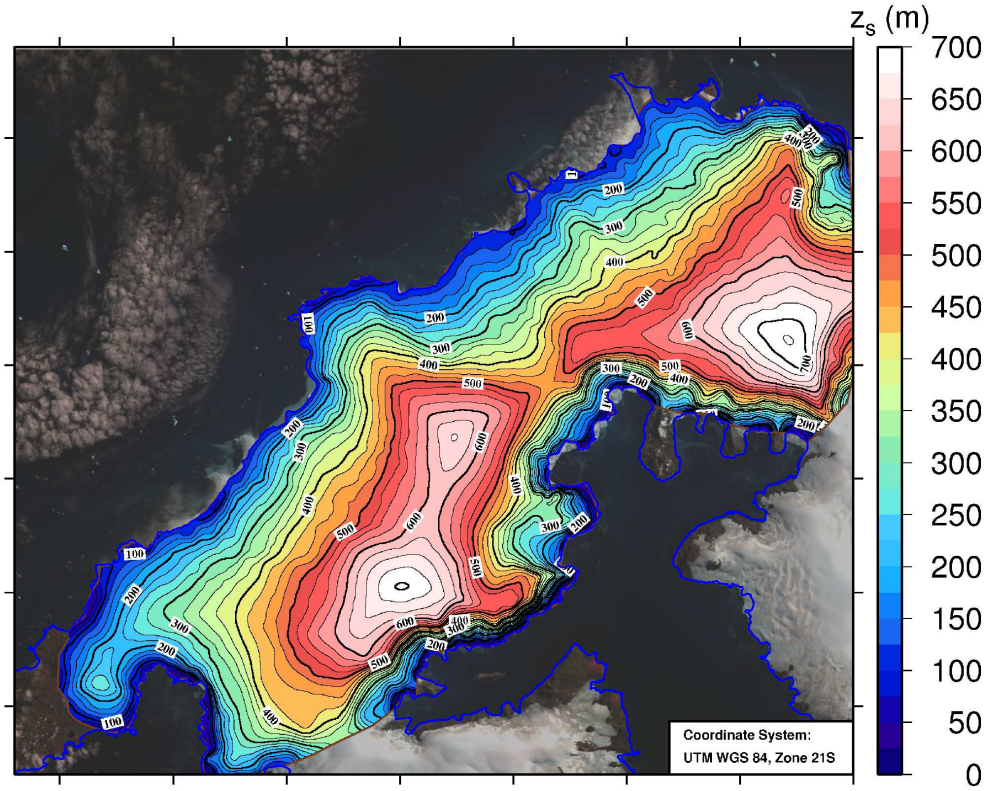

Fig. 5. DEM of the interpolated ice surface topography z_s in m (WGS84) on King George Island (the contour line interval is 25 m). Database: compilation of the groundbased survey (taken from Blindow et al., 2010) and the airborne measurements. Background image is a © SPOT Image from 2000.

ESSDD
4, 123–139, 2011

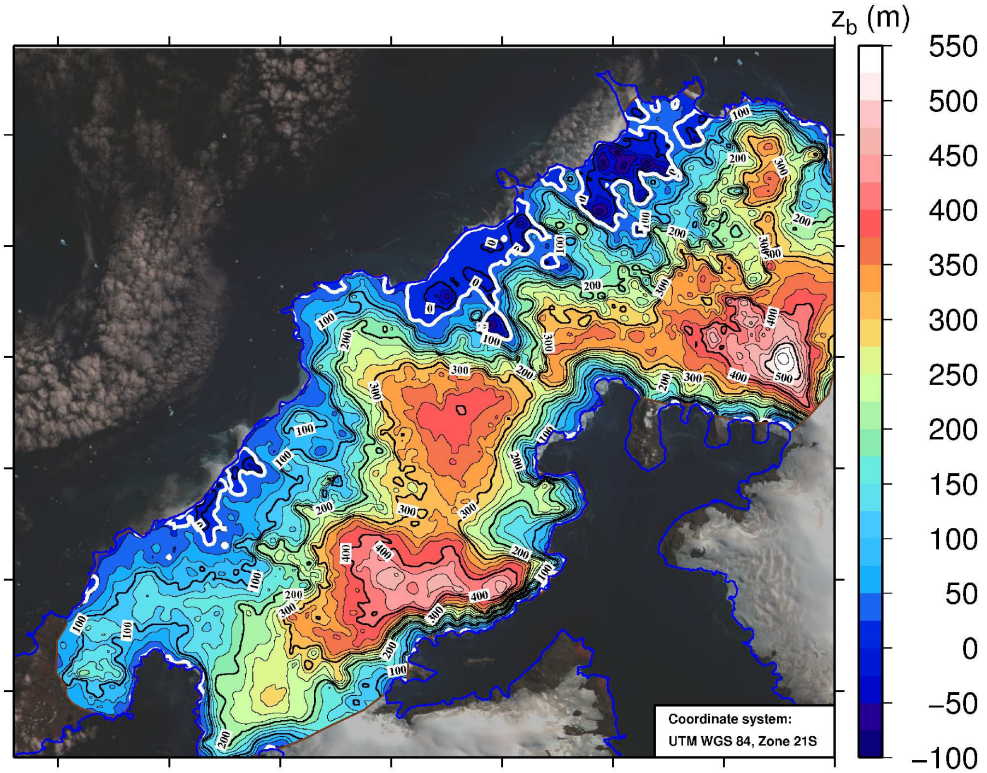

Fig. 6. DEM of the calculated bedrock topography z_b in m (WGS84) on King George Island (the contour line interval is 25 m). The white thick line bordered areas below sea level (details see main text). Database: compilation of the groundbased survey (taken from Blindow et al., 2010) and the airborne measurements. Background image is a ©SPOT Image from 2000.

ESSDD
4, 123–139, 2011